Biomimetics of the [FeFe]-hydrogenase enzyme: Identification of kinetically favoured apical-basal $[Fe_2(CO)_4(\mu\text{-}H)\{\kappa^2\text{-}Ph_2PC(Me_2)PPh_2\}(\mu\text{-}pdt)]^+$ as a proton-reduction catalyst

Shishir Ghosh[a], Ben E. Sanchez[a], Idris Richards[a], Mohammed N. Haque[a], Katherine B. Holt[a], Michael G. Richmond[b*] and Graeme Hogarth[c*]

[a] *Department of Chemistry, University College London, 20 Gordon Street, London, WC1H 0AJ, U.K*

[b] *Department of Chemistry, University of North Texas, 1155 Union Circle, Box 305070, Denton, Texas 76203, USA. Email: cobalt@unt.edu*

[c] *Department of Chemistry, King's College London,, Britannia House, 7 Trinity Street, London SE1 1DB, UK. Email: graeme.hogarth@kcl.ac.uk*

ABSTRACT: Reaction of $[Fe_2(CO)_6(\mu\text{-}pdt)]$ with the small bite-angle diphosphine 2,2′-bis(diphenylphosphino)propane gave the chelated complex $[Fe_2(CO)_4\{\kappa^2\text{-}Ph_2PC(Me_2)PPh_2\}(\mu\text{-}pdt)]$. This exists in solution as a mixture of non-interconverting dibasal and apical-basal isomers which slowly rearrange to the bridged isomer, $[Fe_2(CO)_4\{\mu\text{-}Ph_2PC(Me_2)PPh_2\}(\mu\text{-}pdt)]$, upon heating. X-ray structures of the dibasal and bridged isomers reveal an increase of *ca.* 19° in the PCP bond angle upon diphosphine movement from chelated to bridged positions. To probe the relative stability of these isomers, DFT calculations have been carried out and the bridged isomer is found to lie 3.8 and 1.3 kJ mol^{-1} lower in energy than the dibasal and apical-basal chelated isomers respectively. Protonation of the bridged isomer with $HBF_4{\cdot}Et_2O$ is slow and gives an unstable product. In contrast, both chelated isomers protonate rapidly and cleanly to initially yield apical-basal $[Fe_2(CO)_4(\mu\text{-}H)\{\kappa^2\text{-}Ph_2PC(Me_2)PPh_2\}(\mu\text{-}pdt)][BF_4]$, which rearranges slowly to the dibasal isomer. The latter has been crystallographically characterized, protonation resulting in only very minor metric changes with the iron-iron bond length and diphosphine coordination being essentially unchanged. Electrochemical studies have been carried out in MeCN, and for the chelated isomers separate redox features are seen for the dibasal and apical-basal isomers. The chelated isomers are proton reduction catalysts in acetonitrile in the presence of $HBF_4{\cdot}Et_2O$. Proton reduction occurs at -1.58 V *via* the kinetically favoured apical-basal hydride cation. DFT calculations have been used to study the mechanism of formation of H_2 and are consistent with competing CECE and CEECC mechanisms, the

branch point being the protonation or one-electron reduction of the 35-electron species $[Fe_2(CO)_4(\mu\text{-}H)\{\kappa^2\text{-}Ph_2PC(Me_2)PPh_2\}(\mu\text{-}pdt)]$.

Keywords: [FeFe]-hydrogenase, diphosphine, dithiolate, diiron, chelating, biomimetic, DFT

Introduction

The sustainable generation of hydrogen as an energy carrier in order to realise a fossil-free economy has prompted enormous interest in the chemistry of dithiolate-bridged diiron complexes as models of the H-cluster active site of [FeFe]-hydrogenases [1]. Prompted by theoretical studies by Tye, Hall and Darensbourg [2] suggesting that asymmetry of the diiron centre was a desirable feature of biomimetic models, we [3-6] and others [7-21] have prepared a range of chelated complexes of the type $[Fe_2(CO)_4(\kappa^2\text{-diphosphine})(\mu\text{-dithiolate})]$ in which the diphosphine discriminates the two iron sites both sterically and electronically. In solution the chelated diphosphine exists in both dibasal (**bb**) and apical-basal (**ab**) forms and in some instances the bridged isomer, $[Fe_2(CO)_4(\mu\text{-diphosphine})(\mu\text{-dithiolate})]$, is also accessible [3-6, 22-27]. Indeed, we have recently prepared and tested as proton reduction catalysts both bridged and chelated isomers of $[Fe_2(CO)_4\{Ph_2PN(allyl)PPh_2\}(\mu\text{-}pdt)]$ (pdt = propanedithiolate), with the chelated isomer showing superior catalytic properties [6]. In light of these results, we have focused our continuing efforts towards functional biomimetics of the H-cluster active site on the preparation of new chelated complexes, $[Fe_2(CO)_4(\kappa^2\text{-diphosphine})(\mu\text{-dithiolate})]$. In earlier work we showed that the small bite-angle diphosphine, bis(diphenylphosphino)methane (dppm), reacts with $[Fe_2(CO)_6(\mu\text{-}pdt)]$ (**1**) to initially afford $[Fe_2(CO)_5(\kappa^1\text{-dppm})(\mu\text{-}pdt)]$, which loses a further carbonyl upon heating to yield $[Fe_2(CO)_4(\mu\text{-dppm})(\mu\text{-}pdt)]$ [4]. On one occasion we also isolated small amounts of the chelated isomer, $[Fe_2(CO)_4(\kappa^2\text{-dppm})(\mu\text{-}pdt)]$, which we were able to crystallographically characterize [4], but we have since not been able to reproduce this result and thus cannot carry out an electrocatalytic study of this complex.

It is known that alkyl substitution of one or more of the backbone protons in dppm results in the formation of ligands that are both more basic and possess a smaller bite angle than dppm, thus favouring chelate formation [28-40]. Both of these features were appealing to us for the preparation of readily protonated $[Fe_2(CO)_4(\kappa^2\text{-diphosphine})(\mu\text{-}pdt)]$ complexes. While a number of backbone-functionalised dppm-derivatives have been reported, they are generally

prepared "on metal" from coordinated dppm upon deprotonation of a backbone proton, followed by quenching with electrophiles [30-33]. Such ligands are not easily prepared "off-metal" as they result from the nucleophilic substitution of dihaloalkanes, $RCHX_2$ or R_2CX_2, by the diphenylphosphide anion, Ph_2P^-. The latter is a poor nucleophile and both the steric and electronic changes to central carbon atom upon alkyl substitution make it less susceptible to nucleophilic attack. Two diphosphines that are accessible *via* this route are the methyl-substituted derivatives, 1,1′-bis(diphenylphosphino)ethane, $Ph_2PCH(Me)PPh_2$ [30] and 2,2′-bis(diphenylphosphino)propane, $Ph_2PC(Me_2)PPh_2$ [30]. The former can be isolated in moderate yields and is relatively air-stable, while the latter is formed in lower yields and is oxygen sensitive, presumably reflecting its greater basicity. Both diphosphines are known to favour chelate complexes [30-40] and thus we have attempted to prepare hydrogenase biomimetics containing these ligands.

Herein we report the successful synthesis of $[Fe_2(CO)_4\{\kappa^2\text{-}Ph_2PC(Me_2)PPh_2\}(\mu\text{-pdt})]$ and investigate its ability to act as a proton reduction catalyst. In solution it exits as a mixture of non-interconverting apical-basal and dibasal isomers that display different oxidation and reduction potentials, a situation that has not previously been reported to our knowledge. Protonation by $HBF_4.Et_2O$ rapidly and cleanly affords the apical-basal hydride-cation $[Fe_2(CO)_4(\mu\text{-H})\{\kappa^2\text{-}Ph_2PC(Me_2)PPh_2\}(\mu\text{-pdt})][BF_4]$, which only slowly converts to the thermodynamically favourable dibasal isomer, and thus we propose that it is the kinetically favoured apical-basal complex which is the active proton reduction species. The experimental work presented throughout is supported and illuminated by DFT calculations that allow a detailed analysis of this system.

Results and discussion

*Synthesis and structural characterization of $[Fe_2(CO)_4\{\kappa^2\text{-}Ph_2PC(Me_2)PPh_2\}(\mu\text{-pdt})]$ (**2**)*

In attempting to prepare a [FeFe]-hydrogenase biomimic of the type $Fe_2(CO)_4\{\kappa^2\text{-PXP}\}(\mu\text{-pdt})$ (where PXP is a small-bite angle diphosphine ligand), we initially studied the reaction of $[Fe_2(CO)_6(\mu\text{-pdt})]$ (**1**) with 1,1′-bis(diphenylphosphino)ethane but the results of these efforts were largely disappointing (see ESI). We then turned our attention to 2,2′-bis(diphenylphosphino)propane and this proved to be far more successful. Thus, when

acetonitrile was added to a mixture of **1**, $Ph_2PC(Me_2)PPh_2$ and $Me_3NO.2H_2O$ in a 1:1:2.5 ratio, the initially orange solution darkened rapidly, becoming nearly black after 30 min. The mixture was heated at 70 ^oC for a further 4 h and after work-up afforded the target chelated complex $[Fe_2(CO)_4\{\kappa^2\text{-}Ph_2PC(Me_2)PPh_2\}(\mu\text{-pdt})]$ (**2**) in 63% yield as a mixture of dibasal (**2bb**) and apical-basal (**2ab**) isomers (Scheme 1). The IR spectrum revealed three terminal carbonyl stretching bands at 2018vs, 1949s and 1896m cm^{-1} consistent with the formulation. In order to fully establish the nature of **2**, an X-ray crystal study was performed, the results of which are displayed in Figure 1 and its caption.

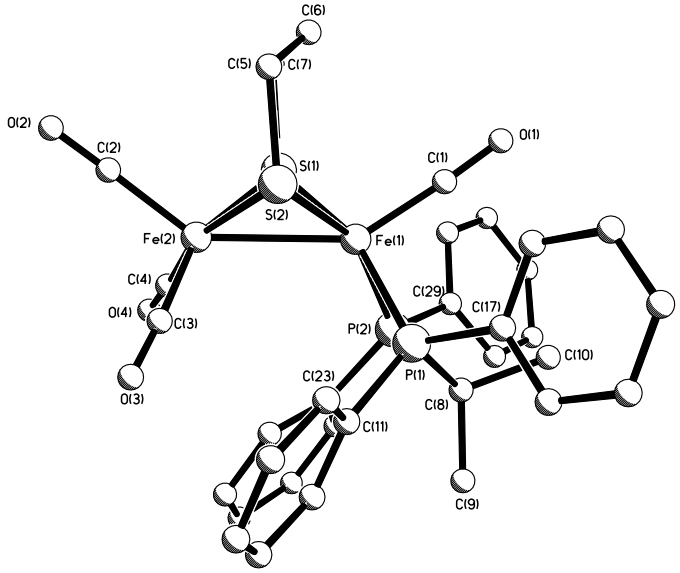

Figure 1. Molecular structure of $[Fe_2(CO)_4\{\kappa^2\text{-}Ph_2PC(Me_2)PPh_2\}(\mu\text{-pdt})]$ (**2bb**) with selected bond lengths (Å) and angles (^{o}): Fe(1)–Fe(2) 2.6062(6), Fe(1)–P(1) 2.2348(6), Fe(1)–P(2) 2.2273(6), Fe(1)–S(1) 2.2270(6), Fe(1)–S(2) 2.2370(5), Fe(2)–S(1) 2.2543(6), Fe(2)–S(2) 2.2706(6), Fe(1)–C(1) 1.747(2), P(1)–Fe(1)–Fe(2) 112.79(2), P(2)–Fe(1)–Fe(2) 108.42(2), C(1)–Fe(1)–Fe(2) 146.19(6), P(1)–Fe(1)–P(2) 74.53(2), P(1)–C(8)–P(2) 90.54(7)

The most interesting feature is the dibasal arrangement of the diphosphine (**2bb** in Scheme 1) with P(1) lying *trans* to S(1) and P(2) *trans* to S(2) [P(1)–Fe(1)–S(1) 163.23(2), P(2)–Fe(1)–S(2) 156.11(2)^o], while the C(1) carbonyl occupies the apical site lying approximately *trans* to the metal-metal vector [C(1)–Fe(1)–Fe(2) 146.19(6)^o]. The diphosphine subtends a bite angle of 74.53(2)^o, which is identical to that of 74.55(4)^o in the analogous dppm-derivative [4], but some 3^o greater than observed in related bis(diphenylphosphino)amine complexes [3,6]. The angle at the backbone carbon in **2** of 90.54(7)^o is significantly smaller than that of 93.5(2)^o in $[Fe_2(CO)_4(\kappa^2\text{-dppm})(\mu\text{-pdt})]$ [4] as a result of the *gem*-dimethyl effect [28-29].

Isomer **2bb** was also examined by DFT and the optimized structure, which is shown in Figure 2, is in agreement with the solid-state structure. Table 1 lists the nature charges and Wiberg indices computed for **2bb**. The Fe_1 and Fe_2 atoms exhibit charges of -1.38 and -1.66, respectively, and the Wilberg bond indices (WBI) for the metal-metal bond is 0.44 being consistent with a formal Fe-Fe bond.

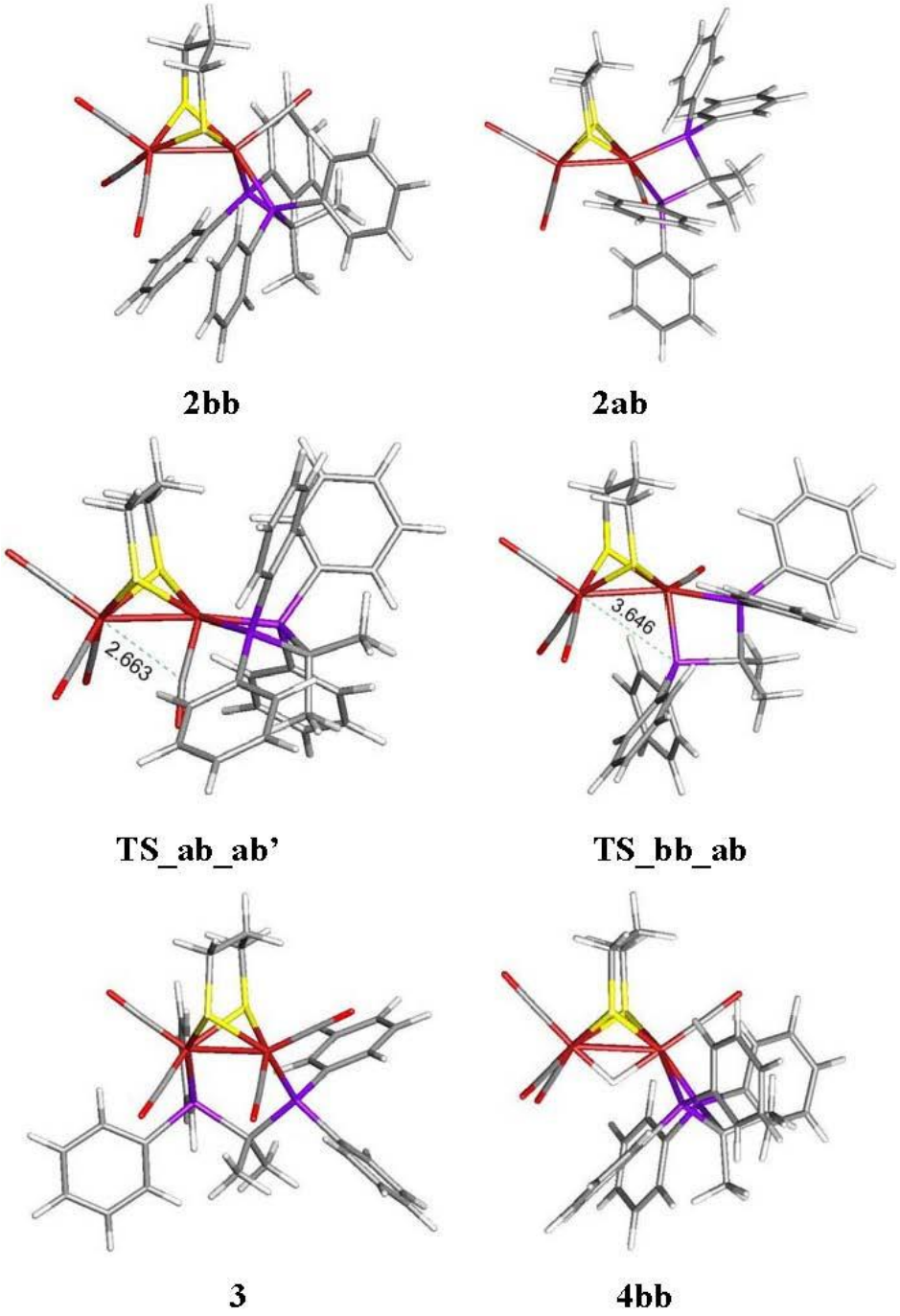

Figure 2. B3LYP-optimized structures for species **2bb**, **2ab**, **3**, **4bb** and transition states **TS_ab_ab'** and **TS_bb_ab**

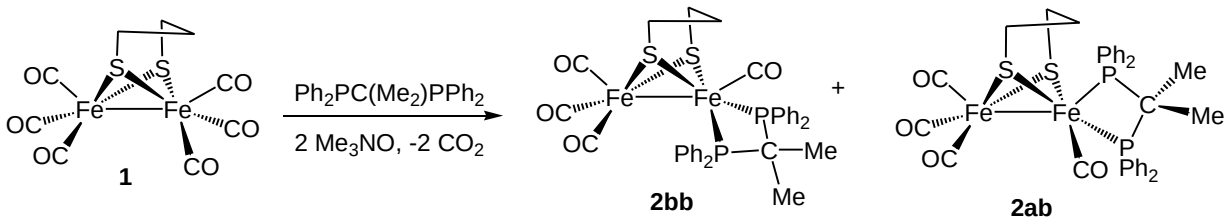

Scheme 1. Synthesis of $[Fe_2(CO)_4\{\kappa^2\text{-}Ph_2PC(Me_2)PPh_2\}(\mu\text{-pdt})]$ (**2**) as a mixture of dibasal (**bb**) and apical-basal (**ab**) isomers

Analysis of the $^{31}P\{^1H\}$ NMR spectrum of the reaction mixture after *ca.* 30 min showed a prominent pair of doublets at 7.6 and 37.2 ppm (J_{PP} 67.5 Hz), which we tentatively assign to intermediate $Fe_2(CO)_5\{\kappa^1\text{-}Ph_2PC(Me_2)PPh_2\}(\mu\text{-pdt})]$, this being supported by the observation of small absorptions at 2045 and 1981 cm^{-1} in the IR spectrum. Thus, it seems that the reaction proceeds in an analogous manner to that observed for dppm [4]. A $^{31}P\{^1H\}$ NMR spectrum in $CDCl_3$ of the crude reaction mixture after 4 h also showed resonances for the chelated isomer, along with a small resonance at 86.9 ppm associated with the bridging isomer (*vide infra*) but this was formed in < 3 % yield.

Relationship between dibasal and apical-basal isomers

The solid-state structure for $[Fe_2(CO)_4\{\kappa^2\text{-}Ph_2PC(Me_2)PPh_2\}(\mu\text{-pdt})]$ is based on the dibasal isomer **2bb**, and attempts to obtain single crystals of the apical-basal isomer (**2ab**) were unsuccessful. In solution dibasal (**2bb**) and apical-basal (**2ab**) isomers co-exist (Scheme 1) as revealed by the presence of two singlets in the $^{31}P\{^1H\}$ NMR spectrum at 52.4 and 77.2 ppm in CD_2Cl_2 (50.8 and 75.5 ppm in $CDCl_3$) in an approximate 2:1 ratio. The $^{31}P\{^1H\}$ NMR chemical shift was assigned to the isomers on the basis of previous work which established that the apical-basal isomer appears downfield of the dibasal isomer [6-11]. The ^1H NMR spectrum is also more complicated than might at first be expected as both isomers have inequivalent methyl groups (all coupled to phosphorus) and either four (dibasal) or six (apical-basal) different protons on the dithiolate backbone. Such isomerism is common in complexes of this type [3-19] with the apical-basal isomer generally being preferred. For example in the dppp analogue of **2**, namely $[Fe_2(CO)_4\{\kappa^2\text{-}Ph_2P(CH_2)_3PPh_2\}(\mu\text{-pdt})]$, the ratio of apical-basal to dibasal isomers is 12:1 [5], although we recently found that for the small bite-angle diphosphine complexes $[Fe_2(CO)_4\{\kappa^2\text{-}Ph_2PN(R)PPh_2\}(\mu\text{-pdt})]$ the dibasal isomer predominated in solution [6].

For the isomeric mixture based on **2**, we have carried out DFT calculations which revealed that the apical-basal isomer **2ab** is lower in energy by 1.3 kJ mol^{-1} than the dibasal form **2bb**; on the basis of this energy difference we predict a K_{eq} of 1.6 which is opposite to the 2:1 ratio of **2bb**:**2ab** found by ^{31}P NMR spectroscopy. In solution at room temperature, a single phosphorus resonance is observed for both isomers. While a single ^{31}P resonance for **2bb** is consistent with the formulated structure having idealized C_s symmetry, the observation of a single phosphorus resonance for **2ab** supports the rapid equilibration of the diphosphine ligand about the Fe(CO)P_2 centre of **2ab** (Scheme 2).

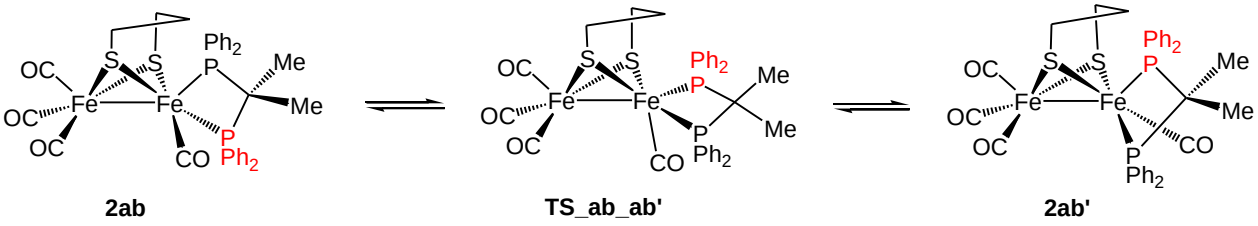

Scheme 2. Low-energy pathway for the interconversion of **2ab** to **2ab′**

DFT calculations confirm a low-energy path (43.9 kJ mol^{-1}) for the degenerate isomerization of **2ab** to **2ab′** through a tripodal rotation at the Fe(CO)P_2 centre. The optimized transition structure **TS_ab_ab′** exhibits a rotated orientation of migrating groups. The activation barrier is sufficiently low and precludes the observation of distinct apical and basal ^{31}P resonances for this isomer. There is no evidence for the interconversion between **2ab**/**ab′** and **2bb** as both sets of signals are sharp at room temperature and remain so upon heating to 90 ^{o}C and DFT calculations give a free energy of activation of 102.6 kJ mol^{-1} (Scheme 3), confirming that the two isomers do not interconvert under the conditions of electrochemical or protonation experiments (see later). The relatively large energy barrier for the isomerization involving **2ab**/**ab′** to **2bb** may be traced to the transition structure **TS_bb_ab′** that requires the adoption of a rotated structure where one of the Ph_2P moieties is situated in an axial position opposite to the pdt ligand. This conformation is energetically unfavorable and places the axial Ph_2P moiety in close contact with the iron-iron bond and the adjacent $Fe(CO)_3$ moiety. This phenomenon is not unlike that reported for the complexes $[Fe_2(CO)_4\{\kappa^2\text{-}Ph_2PN(R)PPh_2\}(\mu\text{-pdt})]$ [6]. The DFT-optimized structures of the two transition states are depicted in Figure 2.

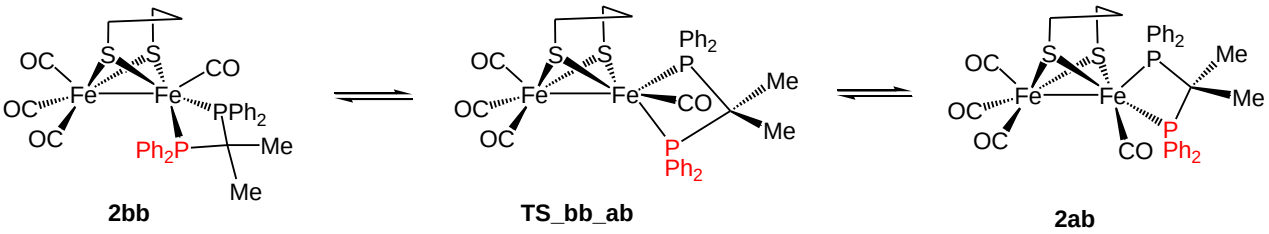

Scheme 3. High-energy pathway for the interconversion of **2ab** to **2bb**

*Synthesis and structural characterization of [$Fe_2(CO)_4${μ-$Ph_2PC(Me_2)PPh_2$}(μ-pdt)] (**3**)*

In recent work we showed that heating chelated complexes [$Fe_2(CO)_4${κ^2-$Ph_2PN(R)PPh_2$}(μ-pdt)] in toluene resulted in their slow (10-14 h) but clean conversion to the bridged isomers [$Fe_2(CO)_4${μ-$Ph_2PN(R)PPh_2$}(μ-pdt)] [6]. After heating a toluene solution of **2** for 8 h it initially appeared that there was no change as shown by IR spectroscopy, but careful inspection of the $^{31}P\{^1H\}$ NMR spectrum revealed the appearance of a small new singlet resonance at *ca.* 89 ppm. Subsequent heating for 30 h resulted in the growth of this resonance and concomitant decrease in intensity of those associated with **2**. Work-up of the reaction mixture at this point led to the isolation of the bridged isomer [$Fe_2(CO)_4${μ-$Ph_2PC(Me_2)PPh_2$}(μ-pdt)] (**3**) in 70% yield (Scheme 4). Characterization was straightforward, the IR spectrum being particularly informative, consisting of four absorptions at 1984m, 1952s, 1916m and 1895sh cm^{-1} typical of a complex of the type [$Fe_2(CO)_4$(μ-diphosphine)(μ-dithiolate)] [4-6,22-27], while the $^{31}P\{^1H\}$ NMR spectrum in CD_2Cl_2 consisted only of a singlet at 89.0 ppm. In order to compare the structure of **3** with that of the chelated isomer, a single crystal X-ray diffraction experiment was carried out, the results of which are summarized in Figure 3 and its caption.

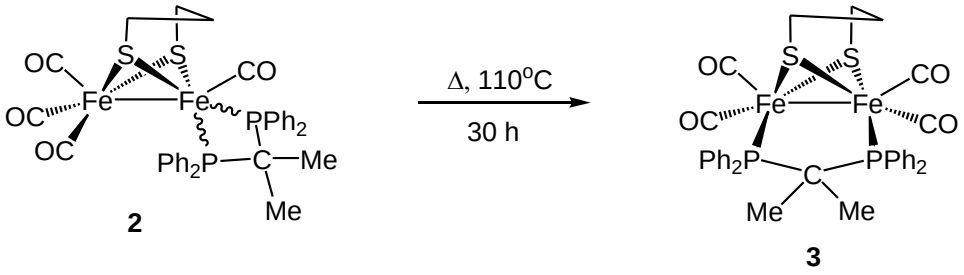

Scheme 4. Synthesis of [$Fe_2(CO)_4${μ-$Ph_2PC(Me_2)PPh_2$}(μ-pdt)] (**3**)

Movement of the diphosphine from a chelated to a bridged disposition results in only very minor changes to the $Fe_2S_2P_2$ core of the molecule. Thus, iron-sulfur and iron-phosphorus bond lengths remain virtually unchanged, while the iron-iron bond length decreases by 0.08 Å (*ca.* 3%). The

biggest change between the two isomers is seen in the angles subtended at the backbone carbon of the 2,2′-bis(diphenylphosphino)propane ligand, for example the P(1)–C(8)–P(2) angle increases from 90.54(7)^{o} in **2** to 107.7(1)^{o} in **3**; a change of around 20% and suggesting that this ligand is quite flexible. As far as we are aware there are only two other examples of crystallographically characterized complexes containing a bridging 2,2′-bis(diphenylphosphino)propane ligand [34,41]. Higgins and co-workers have reported heterobimetallic, [CpRu(μ-CO)$_2${μ-Ph$_2$PC(Me$_2$)PPh$_2$}RhCl$_2$] [34], which has a P–C–P bond angle of 109.9(7)^{o}, and we recently characterized [Os$_3$(CO)$_{10}${μ-Ph$_2$PC(Me$_2$)PPh$_2$}] with a P–C–P bond angle of 111.0(3)^{o} [41].

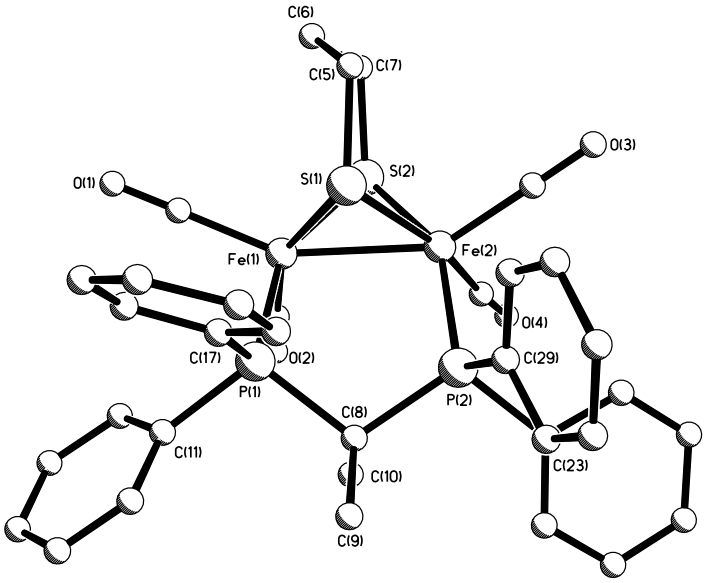

Figure 3. Molecular structure of [Fe$_2$(CO)$_4${μ-Ph$_2$PC(Me$_2$)PPh$_2$}(μ-pdt)] (**3**)·CH$_2$Cl$_2$ with selected bond lengths (Å): Fe(1)–Fe(2) 2.5179(6), Fe(1)–P(1) 2.2352(8), Fe(1)–P(2) 2.2518(8), Fe(1)–S(1) 2.2481(8), Fe(1)–S(2) 2.2508(8), Fe(2)–S(1) 2.2600(8), Fe(2)–S(2) 2.2517(8)

Formation of **3** upon heating the chelated isomers **2** shows that the former is thermodynamically preferred. This was a surprise to us and seems to go against the accepted chelating ability of 2,2′-bis(diphenylphosphino)propane [32-40]. DFT calculations reveal that **3** lies 3.9 and 1.3 kJ mol^{-1} lower in energy than **2bb** and **2ab** respectively (Figure 2). Theoretical investigations showed that unsymmetrically substituted diiron-dithiolate complexes, [Fe$_2$(CO)$_4$L$_2$(μ-dithiolate)], favour the so-called "*rotated*" geometry where a CO ligand asymmetrically bridges the iron-iron vector [1]. DFT analysis of CO substitution by PMe$_3$ in related complexes, namely [Fe$_2$(CO)$_4$(κ^2-dppv)(μ-dithiolate)] [dppv = 1,2-bis(diphenylphosphino)ethylene], showed that the rotation of

the $Fe(CO)_3$ group to form a bridging CO in the transition state is assisted by the electron-rich nature of the Fe(CO)(dppv) fragment [17]. With this in mind, a plausible route for the isomerization process is shown in Scheme 5. This involves migration of a carbonyl from one iron to another *via* a semi-bridging mode followed by rupture of an iron-phosphorus bond to generate the 32-electron complex, $[Fe_2(CO)_4\{\kappa^1\text{-}Ph_2PC(Me_2)PPh_2\}(\mu\text{-pdt})]$. In the latter, once the coordinated diphenylphosphino moiety is in a basal site, then the second phosphine can bridge across to the other iron centre to afford **3**. A similar route has been proposed for the electron-transfer-catalysed (ETC) isomerization of $[Fe_2(CO)_4(\kappa^2\text{-dppe})(\mu\text{-pdt})]$ [9]. However, we cannot rule out the possibility of an iron-sulfur bond scission during CO migration, a process we previously proposed for related amino-diphosphine complexes [6]. Attempts to differentiate between these two processes both experimentally and by DFT calculation have been unsuccessful.

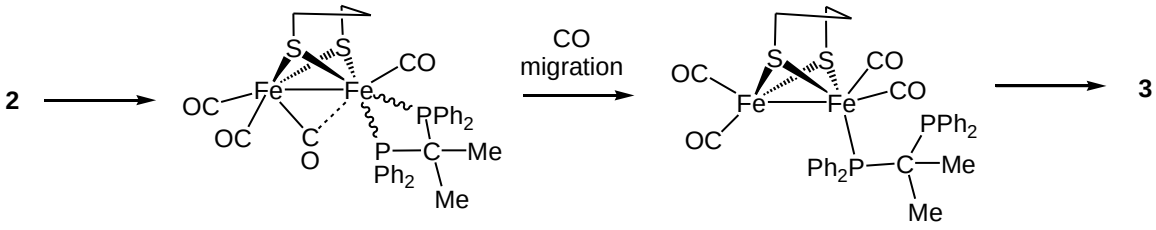

Scheme 5. A proposed mechanism for the conversion of **2** to **3**

Synthesis and structural characterization of $[Fe_2(CO)_4(\mu\text{-}H)\{\kappa^2\text{-}Ph_2PC(Me_2)PPh_2\}(\mu\text{-pdt})][BF_4]$ ***(4)***

Many biomimetic models of the [FeFe]-hydrogenase enzyme bind a proton and this is a key step in the electrocatalytic proton reduction by model systems [42-49]. Thus, we assessed the proton binding ability of **2** and **3**. Addition of $HBF_4{\cdot}Et_2O$ to a dichloromethane solution of **3** resulted only in the slow decomposition of the starting material in an analogous fashion to behaviour noted for $[Fe_2(CO)_4(\kappa^2\text{-dppm})(\mu\text{-pdt})]$ [4]. In contrast, addition of $HBF_4{\cdot}Et_2O$ to $[Fe_2(CO)_4\{\kappa^2\text{-}Ph_2PC(Me_2)PPh_2\}(\mu\text{-pdt})]$ (**2**) resulted in the immediate and clean formation of apical-basal $[Fe_2(CO)_4(\mu\text{-H})\{\kappa^2\text{-}Ph_2PC(Me_2)PPh_2\}(\mu\text{-pdt})][BF_4]$ (**4ab**) which slowly converted (*ca.* 4 h) into the dibasal isomer $[Fe_2(CO)_4(\mu\text{-H})\{\kappa^2\text{-}Ph_2PC(Me_2)PPh_2\}(\mu\text{-pdt})][BF_4]$ (**4bb**) upon standing (Scheme 6). These transformations were easily followed by a combination of NMR and IR spectroscopies. Thus, upon initial addition of $HBF_4{\cdot}Et_2O$ a colour change from red-orange to

blue-green occurred and IR absorptions attributed to **2** were replaced by bands at 2093vs, 2044s and 1982br cm^{-1} associated with **4ab**. Monitoring the same reaction by NMR spectroscopy (in CD_2Cl_2) showed the immediate loss of all signals associated with **2** and formation of a hydride at δ –15.50 (dd, J 18.4, 4.4 Hz) in the ^1H NMR spectrum and two doublets at 68.7 and 60.1 ppm (J_{PP} 62.0 Hz) in the $^{31}P\{^1H\}$ NMR spectrum. Over time these signals diminished and were replaced by a triplet at δ –10.78 (t, J 19.2 Hz) and a singlet at 55.8 ppm in the ^1H and $^{31}P\{^1H\}$ NMR spectra, respectively, associated with **4bb**. Similarly in the IR spectrum, adsorptions associated with **4ab** gradually diminished and were replaced by those at 2097vs, 2048s, 2035s and 1964s cm^{-1} attributed to **4bb**.

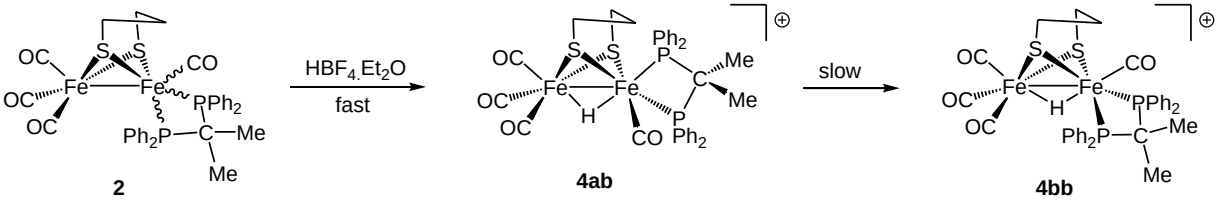

Scheme 6. Reaction $[Fe_2(CO)_4\{\kappa^2\text{-}Ph_2PC(Me_2)PPh_2\}(\mu\text{-pdt})]$ (**2**) with $HBF_4{\cdot}Et_2O$

Single crystals of **4bb** were grown and the results of an X-ray diffraction study are summarized for the diiron cation in Figure 4 and its caption. It co-crystallizes with a disordered molecule of dichloromethane but there are no intermolecular interactions between either this or the BF_4^- anion and the diiron cation and consequently these will not be discussed further. The diiron units in **2bb** and **4bb** are remarkably similar, showing that protonation across the iron-iron vector does not significantly perturb the system; the iron-iron bond length of 2.602(1) Å in **4bb** being within error the same as that seen in **2bb**. Other bond lengths also do not vary significantly upon protonation, while the angles subtended by the bite-angle of the diphosphine of 74.04(4)° and also the angle subtended at the backbone carbon [P(1)–C(8)–P(2) 90.9(2)°] are almost the same as those found in **2bb**. The largest metric changes between the two structures are the bond angles subtended by the basal carbonyl and phosphine groups to the iron-iron bond, all values being greater in **4bb** as a result of the extra room required to accommodate the bridging hydride. For example, Fe(1)–Fe(2)–C(3) and Fe(1)–Fe(2)–C(4) bond angles of 119.3(2) and 110.7(2)° in **4bb** are significantly expanded with respect to those of 106.64(6) and 108.14(6)° respectively in **2bb**. A further noteworthy feature of both **2bb** and **4bb** is the orientation of the dithiolate backbone, the central methylene group being orientated towards the more bulky Fe(CO)(diphosphine) moiety. It is not clear why this should be the case and interestingly in

$[Fe_2(CO)_4(\mu\text{-}H)\{\kappa^2\text{-}Ph_2PN(allyl)PPh_2\}(\mu\text{-}pdt)][BF_4]$ it is orientated towards the $Fe(CO)_3$ sub-unit [5]. It is noteworthy that in crystallographic structures of related diiron pdt complexes the backbone methylene units are often structurally disordered and as such the precise proton positions cannot be accurately located. In both **2bb** and **4bb** there is no evidence of any disorder and this has allowed all these protons to be located from Fourier difference maps and refined. The DFT calculated structure for **4bb** (Figure 2) closely resembles the solid-state structure.

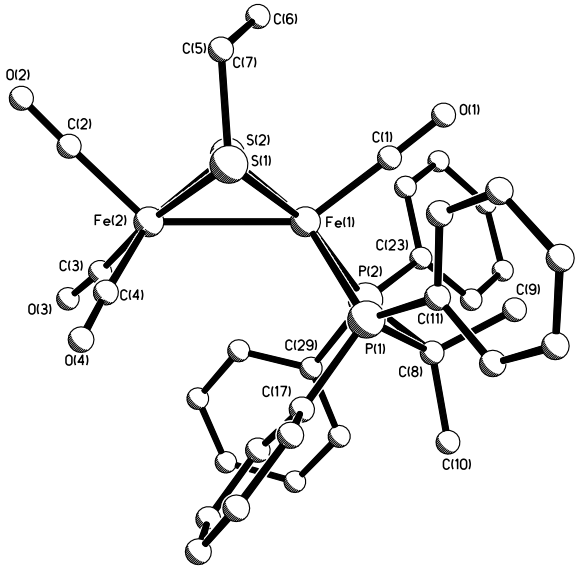

Figure 4. Molecular structure of the diiron cation in $[Fe_2(CO)_4(\mu\text{-}H)\{\kappa^2\text{-}Ph_2PC(Me_2)PPh_2\}(\mu\text{-}pdt)][BF_4].0.5CH_2Cl_2$ (**4bb**).$0.5CH_2Cl_2$ with selected bond lengths (Å) and angles (°): Fe(1)–Fe(2) 2.602(1), Fe(1)–P(1) 2.226(1), Fe(1)–P(2) 2.254(1), Fe(1)–S(1) 2.251(1), Fe(1)–S(2) 2.251(1), Fe(2)–S(1) 2.269(1), Fe(2)–S(2) 2.273(1), Fe(1)–C(1) 1.756(4), P(1)–Fe(1)–Fe(2) 114.51(4), P(2)–Fe(1)–Fe(2) 119.55(4), C(1)–Fe(1)–Fe(2) 142.5(1), P(1)–Fe(1)–P(2) 74.04(4), P(1)–C(8)–P(2) 90.9(2)

The clean and rapid protonation of both **2ab** and **2bb** to give **4ab** is somewhat surprising as the two isomers do not interconvert at room temperature. Further, the absence of **4bb** immediately after protonation suggests that the reaction proceeds *via* a common unobserved intermediate that partitions to the apical-basal hydride **4ab** under kinetically controlled conditions. The latter assertion was confirmed by DFT calculations, which reveal that **4bb** is 17 kJ mol^{-1} more stable than **4ab**. In previous work with an analogue of **2**, namely $[Fe_2(CO)_4\{\kappa^2\text{-}Ph_2P(CH_2)_3PPh_2\}(\mu\text{-}pdt)]$, a similar situation was observed i.e. the mixture of apical-basal and dibasal isomers (12:1) immediately converted to apical-basal $[Fe_2(CO)_4(\mu\text{-}H)\{\kappa^2\text{-}Ph_2P(CH_2)_3PPh_2\}(\mu\text{-}pdt)][BF_4]$ upon

addition of $HBF_4{\cdot}Et_2O$ [5]. Indeed when we carried out the protonation at -90°C we observed the intermediate formation of a terminal hydride. Unfortunately all attempts to observe similar low-temperature species upon protonation of **2** were unsuccessful. However, it seems reasonable to suggest that a common intermediate is also formed here, protonation of both **2ab** and **2bb** initially yielding $[HFe_2(CO)_4\{\kappa^2\text{-}Ph_2PC(Me_2)PPh_2\}(\mu\text{-pdt})][BF_4]$ (**4tH**). The structure of **4tH** is not known but by analogy to the dppp-chemistry the hydride is most probably attached to the iron which is chelated by the diphosphine occupying both the basal sites with a carbonyl at apical position [5]. We further note that as found by ourselves [5] and others [8] for the analogous dppp-hydride, apical-basal $[Fe_2(CO)_4(\mu\text{-H})\{\kappa^2\text{-}Ph_2P(CH_2)_3PPh_2\}(\mu\text{-pdt})][BF_4]$, **4ab** is not deprotonated upon addition of strong bases, which shows that proton and ligand rearrangements are intramolecular.

*Cyclic voltammetry studies of $[Fe_2(CO)_4\{\kappa^2\text{-}Ph_2PC(Me_2)PPh_2\}(\mu\text{-pdt})]$ (**2**) and $[Fe_2(CO)_4\{\mu\text{-}Ph_2PC(Me_2)PPh_2\}(\mu\text{-pdt})]$ (**3**)*

The CV of **2** in MeCN at scan rate 0.1 Vs^{-1} is shown in Figure 5. Two quasi-reversible oxidation waves are seen at $E_{1/2}$ = –0.19 V (ΔE = 110 mV) and $E_{1/2}$ = 0.04 V (ΔE = 80 mV), the reversibility of which is maintained at all scan rates, together with a further irreversible oxidation at E_p = 0.66 V. In the cathodic domain, two overlapping reductive features are observed at E_p = –2.16 V and E_p = –2.23 V together with a third quasi-reversible reduction at $E_{1/2}$ = –2.45 V (ΔE = 70 mV). The two overlapping reduction peaks also show some reversibility at all scan rates, becoming more separated at higher scan rates (≥ 0.25 V/s) (Figure 6). After reduction, a series of small oxidative features are observed between –2.0 to –1.3 V and 0.23 V on the return scan, which are due to the oxidation of products formed upon first and second reductions (Figure S1). The plot of peak current (i_p) vs. square root of scan rate ($\sqrt{v}$) gives straight line for all primary oxidative and reductive processes, suggesting that all redox events of **2** are diffusion-controlled (Figure S2).

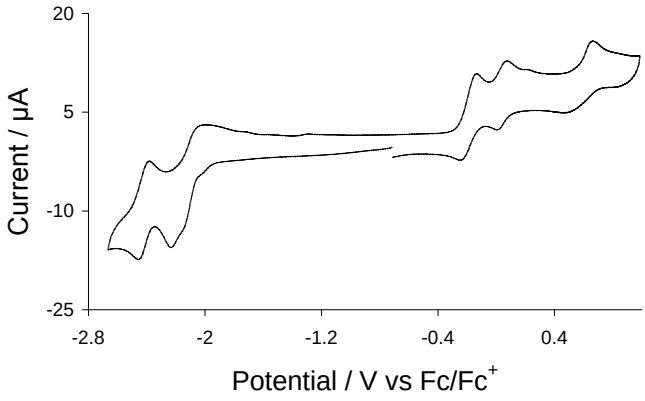

Figure 5. CV of $[Fe_2(CO)_4\{\kappa^2\text{-}Ph_2PC(Me_2)PPh_2\}(\mu\text{-pdt})]$ (**2**) in MeCN (0.5 mM solution, supporting electrolyte $[NBu_4][PF_6]$, scan rate 0.1 Vs^{-1}, glassy carbon electrode, potential vs Fc^+/Fc).

Schollhammer and Talarmin reported that diiron-dithiolate complexes containing a chelating dppe ligand undergo electron-transfer-catalysed isomerization upon one-electron reduction to form the symmetrical isomers in which the dppe bridges the iron-iron vector [9]. We did not see any evidence of such isomerization for **2**. If **2** converted into **3** after reduction, then we would see peak(s) in the anodic region for **3** on the return scan, but we obtained identical CVs by sweeping the voltage in opposite directions (scanning anodic or cathodic region first) even in slower scan rates (Figure S3). This suggests that **2** is not converting into **3** after reduction at least on the voltammetric time-frame.

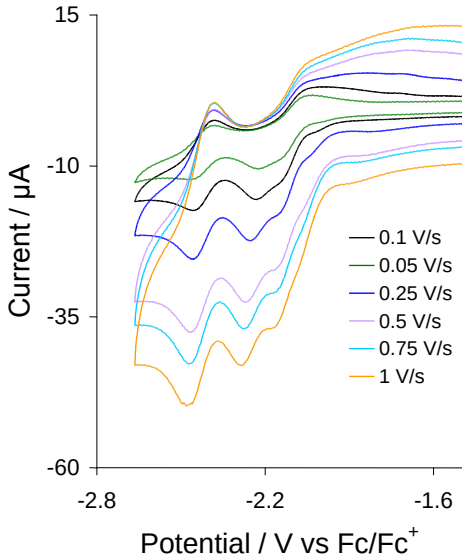

Figure 6. CVs of $[Fe_2(CO)_4\{\kappa^2\text{-}Ph_2PC(Me_2)PPh_2\}(\mu\text{-pdt})]$ (**2**) at various scan rates as shown in the legend (in MeCN, 0.5 mM solution, supporting electrolyte $[NBu_4][PF_6]$, glassy carbon electrode, potential vs Fc^+/Fc)

The voltammetry of the related $[Fe_2(CO)_4\{\kappa^2\text{-}Ph_2PN(allyl)PPh_2\}(\mu\text{-pdt})]$ species showed a lack of reversibility of both oxidation and reduction processes in MeCN [6]. Additionally, the second oxidation peak for the complex occurred ca. 0.5 V more positive than the first oxidation, unlike the response noted for **2**, where two overlapping, reversible oxidation peaks are observed. Likewise only one irreversible reduction peak was seen for $[Fe_2(CO)_4\{\kappa^2\text{-}Ph_2PN(allyl)PPh_2\}(\mu\text{-pdt})]$, in contrast to the two closely spaced, reversible reduction peaks for **2**. One interpretation for this observation is that the two oxidation and reduction peaks arise from separate one-electron oxidation and reduction of the two geometric isomers of **2**, namely **2ab** and **2bb**. It is not possible to unambiguously assign individual oxidation and reduction waves to specific isomers although DFT calculations shed some light on these processes. Thus, the HOMO of the dibasal isomer **2bb** is some 0.0067 Hartrees (0.18 eV, 17.6 kJ mol^{-1}) higher in energy than that in **2ab**. Thus we suggest that the first oxidation is associated with electron loss from **2bb** and the second oxidation wave attributed to **2ab**. The energy difference between the two LUMOs is small and **2ab** lies 0.0016 Hartrees (0.04 eV, 4.30 $kJmol^{-1}$) below the LUMO of **2bb** thus accounting for the two reduction waves and suggesting that the reduction at less negative potential is associated with **2ab**. The CV behavior recorded for **2** may result from overlap of the separate waves from both isomers. As far as we are aware, the separate and distinguishable oxidation and reduction waves for dibasal and apical-basal isomers have not previously been noted [6,9,14-16]. The reversibility of the responses suggests that both the mixed valence state complexes, Fe(II)-Fe(I) $[Fe_2(CO)_4\{\kappa^2\text{-}Ph_2PC(Me_2)PPh_2\}(\mu\text{-pdt})]^+$ ($\mathbf{2}^+$) and Fe(I)-Fe(0) $[Fe_2(CO)_4\{\kappa^2\text{-}Ph_2PC(Me_2)PPh_2\}(\mu\text{-pdt})]^-$ ($\mathbf{2}^-$) are reasonably long-lived. The latter is especially important with respect to the electrocatalytic reduction of protons and is considered in detail in the next section.

For comparison we have also studied the CV of the thermodynamically favoured bridged isomer **3** in MeCN (Figure S4). Due to its low solubility in this solvent the sample was sonicated and heated for some time to aid dissolution. Consequently, the precise concentration used was not determined, but nevertheless the data provide a useful comparison with those for **2**. The CV displays a reduction at E_p = –2.50 V and an oxidation at E_p = 0.74 V both of which show some reversibility at this scan rate (0.1 Vs^{-1}), however, neither improved when the scan rate was increased.

*Proton reduction catalysed by **2***

CVs of **2** recorded after addition of molar equivalents of $HBF_4{\cdot}Et_2O$ are shown in Figure 8, which show a positive shift of reduction potentials due to protonation of the initial complex. In light of the protonation studies discussed above, we conclude that under these conditions the major component of the electrochemical cell is apical-basal $[Fe_2(CO)_4(\mu\text{-}H)\{\kappa^2\text{-}Ph_2PC(Me_2)PPh_2\}(\mu\text{-}pdt)][BF_4]$ [**4ab = $Fe_2(H)^+$**]. The first and second reduction waves now appear at E_p = –1.58 V and E_p = –1.88 V, followed by a series of reductive features at more negative potentials. The peak current of these reduction waves increases consistently with addition of each molar equivalent of acid characteristic of electrocatalytic proton reduction by **2** at these potentials.

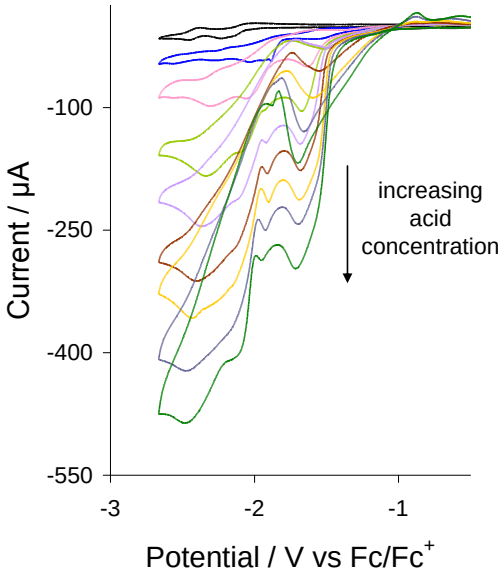

Figure 7. CVs of $[Fe_2(CO)_4\{\kappa^2\text{-}Ph_2PC(Me_2)PPh_2\}(\mu\text{-}pdt)]$ (**2**) in the absence of acid and in the presence of 1-7 and 9 molar equivalents of $HBF_4{\cdot}Et_2O$ (0.5 mM solution, in acetonitrile, supporting electrolyte $[NBu_4][PF_6]$, scan rate 0.1 Vs^{-1}, glassy carbon electrode, potential vs Fc^+/Fc)

Two catalytic pathways have been probed by DFT as summarized in Scheme 7. All of the species involved in those catalytic cycles represent fully optimized ground-state minima (Figure 8). The cationic hydride **$Fe_2(H)^+$** is key to both cycles and its formation derives from the rapid protonation of **2**. Since protonation studies show that there is no further proton addition to this species, we suggest that the next step is a one-electron reduction which takes place at

around –1.58 V (Figure S4) to afford the neutral 35-electron hydride **$Fe_2(H)$** [50]. At this point it is not clear whether a second protonation to give **$Fe_2(H_2)^+$**, or one-electron reduction to yield **$Fe_2(H)^-$** occurs. Certainly, the basicity of **$Fe_2(H)$** should be similar to that of **2ab** and thus we expect this pathway to be favoured, and while reduction of **$Fe_2(H)$** occurs necessarily at a higher potential to that of **4ab** the precise value is not known. DFT calculations show that the 35-electron cationic dihydrogen species **$Fe_2(H_2)^+$** formed by protonation of the neutral hydride **$Fe_2(H)$** is able to release H_2 and gives the radical cation **$2ab^{\bullet+}$**; reduction of the latter species regenerates **2**.

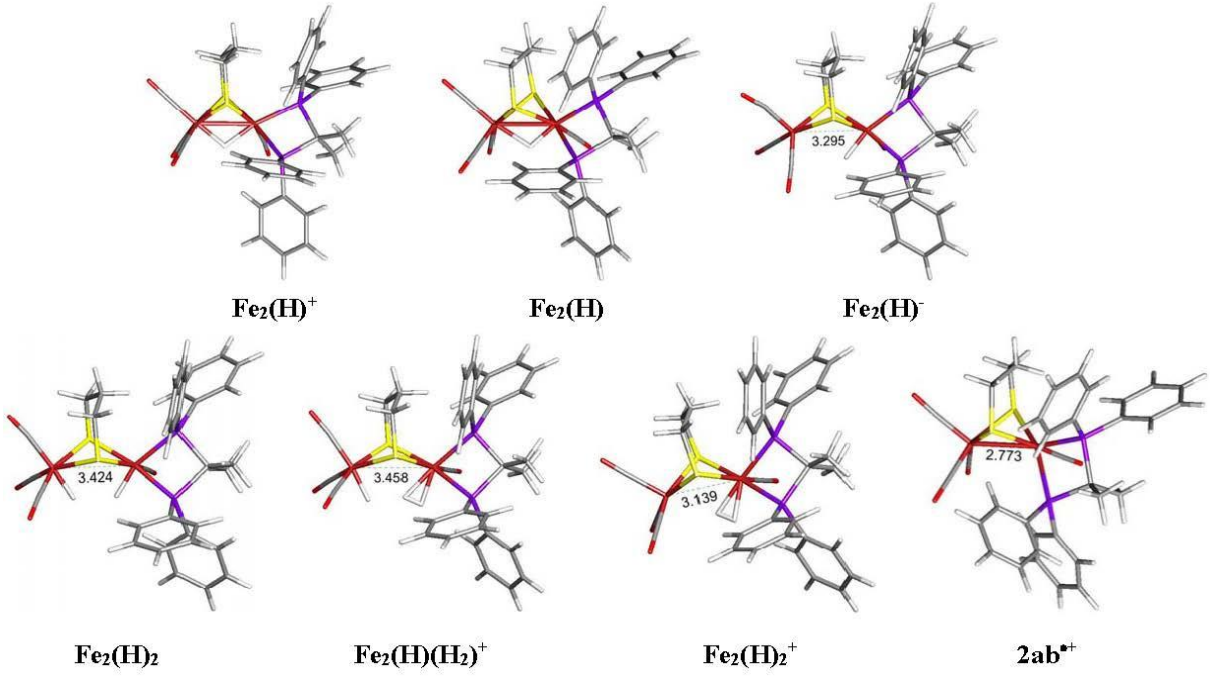

Figure 8. B3LYP-optimized structures for selected intermediates depicted in Scheme 7

Table 1 lists the computed natural charges and Wiberg bond indices (WBI). Protonation of **2ab** to give **$Fe_2(H)^+$** does not lead to a significant change in the natural charges for the Fe, P, and S atoms but does lead to an elongation of the Fe-Fe bond as revealed by a change in the Wiberg index from 0.46 to 0.30. This trend is consistent with a weakening of the Fe-Fe bond upon protonation. Reduction of **$Fe_2(H)^+$** to give **$Fe_2(H)$** is accompanied by a further diminution of the Fe-Fe bond based on the WBI of 0.16. The bridging hydride asymmetrically spans the Fe-Fe vector in the neutral radical given the Fe-H WBIs of 0.54 and 0.23. Here the former index, which contains the dppmMe_2-substituted iron centre, is *ca*. 2.3 times stronger than the Fe-H bond from the $Fe(CO)_3$ moiety. The formation of the molecular hydrogen complex **$Fe_2(H_2)^+$**

may be viewed as a formal protonation of the hydride ligand in **$Fe_2(H)$** and this is accompanied by a further elongation of the Fe-Fe bond, yielding a WBI of 0.07. The coordinated H_2 ligand in **$Fe_2(H_2)^+$** exhibits a mean WBI of 0.29 for the two Fe-H bonds and an index of 0.59 for the H-H bond.

The second pathway propagates *via* reduction of the neutral hydride **$Fe_2(H)$** to form **$Fe_2(H)^-$**, which reacts with an additional proton to generate the 36-electron dihydride **$Fe_2(H_2)$**. The formation of the anionic hydride greatly weakens the Fe-Fe bond (WBI = 0.06) and promotes the formation of a terminal hydride at the $Fe(CO)P_2$ moiety, whose Fe_1-H_1 WBI is 0.72 and significantly stronger than the Fe_2-H_1 index of 0.02. Protonation of **$Fe_2(H)^-$** next occurs at the $Fe(CO)_3$ centre to give the traditional dihydride species **$Fe_2(H)_2$**. The cleavage of the Fe-Fe bond in going from **2** to **$Fe_2(H)_2$** is a formal two-electron reduction process that is consistent Polyhedral Skeletal Electron Pair (PSEP) theory [51]. This species undergoes a third protonation to form **$Fe_2(H)(H_2)^+$**, which releases H_2 and regenerates the cationic hydride **$Fe_2(H)^+$**. The outcome of protonation of **$Fe_2(H)_2$** is akin to the step that furnishes **$Fe_2(H_2)^+$**, insomuch that the H_2 ligand is coordinated to the $Fe(CO)P_2$ centre. The terminal Fe_2-H_2 bond in **$Fe_2(H)(H_2)^+$** is considerably stronger (WBI = 0.73) as compared to the two Fe_1-$H_{1,3}$ bonds for the ligated H_2 ligand that exhibit a mean WBI of 0.30 for the Fe_1-H bonds. The WBI for the H_1-H_3 bond of H_2 is 0.59 and identical to that computed for molecular H_2 ligand in **$Fe_2(H_2)^+$**.

Finally, the DFT calculations also show that **$Fe_2(H_2)^+$** can undergo reduction before release of H_2 to form the dihydride species **$Fe_2(H_2)$**. The reduction process promotes the formal cleavage of the Fe-Fe bond and activation of the coordinated H_2 molecule. One complication to these catalytic pathways is the possible formation of **4bb** during the electrocatalysis. While we cannot completely rule this out, the relatively rapid scan speeds 0.1 Vs^{-1} utilised, as compared with the rate of conversion of **4ab** to **4bb** ($t_{1/2}$ *ca.*1h), would suggest that the amount of **4bb** is always small (less than 1%).

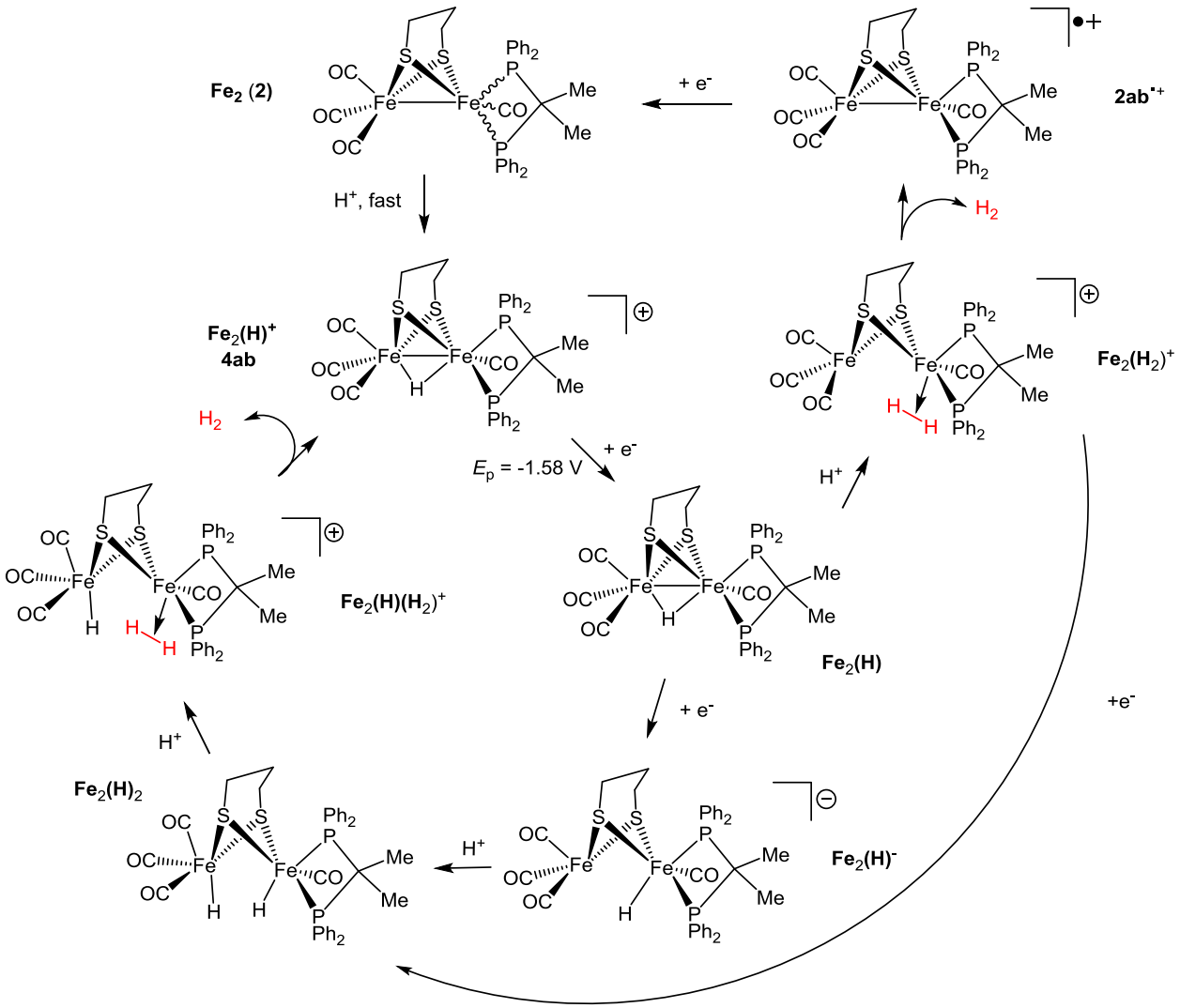

Scheme 7. DFT computed catalytic mechanism for the electrocatalytic proton reduction by $[Fe_2(CO)_4\{\kappa^2\text{-}Ph_2PC(Me_2)PPh_2\}(\mu\text{-pdt})]$ (**2**)

Conclusions

We have detailed the synthesis, structure, and thermal stability of the diphosphine-chelated isomers of $[Fe_2(CO)_4\{\kappa^2\text{-}Ph_2PC(Me_2)PPh_2\}(\mu\text{-pdt})]$ (**2**), together with catalytic studies carried out to assess its proton reduction ability. The X-ray structure shows that **2** adopts the dibasal configuration in the solid state, while both dibasal and apical-basal isomers are found to exist in solution in an approximate 2:1 ratio. The apical-basal isomer **2ab** lies 1.3 kJmol^{-1} lower in energy than the dibasal form **2bb**, and they do not interconvert in solution at room temperature

for which an activation barrier of 102.6 kJ mol^{-1} has been computed. Complex **2** very slowly converts into the bridged isomer **3** upon heating and this provides support that the latter isomer is thermodynamically favoured. DFT calculations show that **3** lies 3.8 and 1.3 kJ mol^{-1} lower in energy than **2bb** and **2ab**, respectively.

Complex **2** undergoes rapid protonation by $HBF_4{\cdot}Et_2O$ to afford initially the apical-basal hydride $[Fe_2(CO)_4(\mu\text{-}H)\{\kappa^2\text{-}Ph_2PC(Me_2)PPh_2\}(\mu\text{-}pdt)][BF_4]$ (**4ab**), which then slowly transforms into the dibasal isomer $[Fe_2(CO)_4(\mu\text{-}H)\{\kappa^2\text{-}Ph_2PC(Me_2)PPh_2\}(\mu\text{-}pdt)][BF_4]$ (**4bb**) upon standing. In contrast the bridged isomer **3** protonates only slowly and the product is unstable, thus ruling it out as a viable proton reduction catalyst. In both chelated hydrides **4ab** and **4bb**, the hydride spans the iron-iron bond but protonation is believed to proceed *via* a fleeting terminal hydride species, namely $[HFe_2(CO)_4\{\kappa^2\text{-}Ph_2PC(Me_2)PPh_2\}(\mu\text{-}pdt)][BF_4]$ (**4tH**). The CV of **2** in MeCN shows separate redox features for both apical-basal and dibasal isomers leading to common intermediates, while that of the bridged isomer displays single oxidative and reductive features. To our knowledge, **2** is the first phosphine-substituted diiron chelate that shows separate redox features for the dibasal and apical-basal isomers. Electrocatalytic studies carried out with **2** in presence of $HBF_4{\cdot}Et_2O$ show that it catalyzes proton reduction following a chemically initiated CE route. An important finding is that it is the kinetic isomer **4ab** is active in the catalytic cycle. DFT methods were applied to probe this mechanism and two interconnected catalytic pathways, namely CECE and CEECC, have been computed to be operative for the catalytic production of H_2. This work thus provides further justification for the development of chelated complexes of the type $[Fe_2(CO)_4(\kappa^2\text{-diphosphine})(\mu\text{-dithiolate})]$ as viable proton reduction catalysts.

Experimental section

General methods and materials

All reactions were carried out using standard Schlenk-line techniques under N_2 and reaction solvents were purified on alumina columns. Work-up was carried out in air using standard bench reagents. The diphosphines $Ph_2PCH(Me)PPh_2$ and $Ph_2PC(Me)_2PPh_2$ [30] and $[Fe_2(CO)_6(\mu\text{-}pdt)]$ (**1**) [52] were prepared by literature procedures. NMR spectra were recorded on a Bruker AMX400 spectrometer and referenced internally to the residual solvent peak (^1H) or externally to $P(OMe)_3$ (^{31}P). Infrared spectra were recorded on a Nicolet 205 FT-

IR spectrometer in a solution cell fitted with calcium fluoride plates, subtraction of the solvent absorptions being achieved by computation. All IR spectra were recorded in CH_2Cl_2 unless otherwise noted. Fast atom bombardment mass spectra were recorded on a VG ZAB-SE high resolution mass spectrometer and elemental analyses were performed in-house at UCL.

*Synthesis of [$Fe_2(CO)_4\{\kappa^2$-$Ph_2PC(Me_2)PPh_2\}(\mu$-pdt)}] (**2**)*

A mixture of **1** (0.20 g, 0.52 mmol), $Ph_2PC(Me_2)PPh_2$ (0.21 g, 0.52 mmol) and $Me_3NO{\cdot}2H_2O$ (0.15 g, 0.14 mmol) were dissolved in MeCN (*ca.* 35 mL). The orange solution darkened rapidly and became black. After stirring for 4 h the solvent was removed under reduced pressure to give a dark red residue. This was washed with hexane (*ca.* 3 x 5 ml) in order to remove any unreacted **1** and diphosphine and the red residue was dried. This was extracted with diethyl ether (*ca.* 20 mL) and cooled to –10 ^oC to afford **2** (0.24 g, 63%) as a brick red powder. Crystals suitable for X-ray diffraction analysis were grown upon slow diffusion of hexanes into a concentrated CH_2Cl_2 solution containing **2**. IR ν(CO): 2018vs, 1949s, 1896m cm^{-1}. $^{31}P\{^1H\}$ NMR ($CDCl_3$): δ 75.5 (s), 50.8 (s); (CD_2Cl_2) 77.2 (s, **2ab**), 52.4 (s, **2bb**) ppm. ^1H NMR (CD_2Cl_2): δ 7.87 – 7.23 (m, 20H, Ph, **2ab** + **2bb**), 3.16 (d, J 6.3, 1H, CH_2, **2ab**), 2.42 (m, 4H, CH_2, **2bb**), 2.15 (brm, 5H, CH_2, **2ab**), 1.94 (br m, 2H, CH_2, **2bb**), 1.85 (t, J 12.2, 3H, Me, **2bb**), 1.82 (t, J 10.7, 3H, Me, **2ab**), 1.38 (t, J 10.8, 3H, Me, **2ab**), 1.34 (t, J 16.8, 3H, Me, **2bb**). Elemental analysis calc. for $Fe_2S_2P_2O_4C_{34}H_{32}$ (found): C 54.99 (55.08), H 4.31 (4.57). Crystallographic data for **2bb**: red block, dimensions 0.36 × 0.16 × 0.13 mm^3, triclinic, space group *P*1bar, a = 10.625(2), b = 11.308(2), c = 15.007(3) Å, α = 86.626(3), β = 81.950(3), γ = 65.000(3)^o, V = 1618.0(5) $Å^3$, Z = 2, F(000) 764, d_{calc} = 1.524 g cm^{-3}, μ = 1.163 mm^{-1}. 13806 reflections were collected, 7330 unique [R(int) = 0.0271]. At convergence, R_1 = 0.0306, wR_2 = 0.0788 [$I > 2.0\sigma(I)$] and R_1 = 0.0337, wR_2 = 0.0804 (all data), for 525 parameters.

*Synthesis of [$Fe_2(CO)_4\{\mu$-$Ph_2PC(Me_2)PPh_2\}(\mu$-pdt)}] (**3**)*

A toluene solution (80 ml) of **2** (0.05 g, 0.67 mmol) was heated at reflux for approximately 30 h. After cooling to room temperature volatiles were removed on a rotary evaporator giving an oily red solid. This was washed with hexane (*ca.* 3 x 5 mL) to give a dry orange solid. The

crude material was dissolved in a minimum amount of CH_2Cl_2 and layered with hexanes to afford large red crystals of **3** (0.035 g, 70%). IR ν(CO): 1984m, 1952s, 1916m, 1895sh cm^{-1}. $^{31}P\{^1H\}$ NMR ($CDCl_3$): δ 86.9 (s); (CD_2Cl_2) 89.0 (s) ppm. ^1H NMR ($CDCl_3$): δ 8.02 – 6.79 (m, 20H, Ph), 2.13 (br, 4H, CH_2), 1.86 (br, 2H, CH_2), 1.65 (t, J 12.7, 3H, Me), 0.86 (m, 3H, Me). Elemental analysis calc. for $Fe_2S_2P_2O_4C_{34}H_{32}.CH_2Cl_2$ (found): C 48.92 (48.66), H 4.20 (4.23). Crystallographic data for **3**·CH_2Cl_2: red block, dimensions 0.34 × 0.32 × 0.21 mm^3, monoclinic, space group $P2_1/n$, a = 12.100(2), b = 21.513(3), c = 13.203(2) Å, α = 90, β = 97.843(2), γ = 90°, V = 3404.7(9) $Å^3$, Z = 4, F(000) 1662, d_{calc} = 1.579 g cm^{-3}, μ = 1.226 mm^{-1}. 28679 reflections were collected, 8100 unique [R(int) = 0.0339]. At convergence, R_1 = 0.0492, wR_2 = 0.1369 [$I > 2.0\sigma(I)$] and R_1 = 0.0545, wR_2 = 0.1414 (all data), for 421 parameters.

*Synthesis of $[Fe_2(CO)_4(\mu\text{-}H)\{\kappa^2\text{-}Ph_2PC(Me)_2PPh_2\}(\mu\text{-}pdt)\}][BF_4]$ (**4**)*

To a CH_2Cl_2 (5 mL) of **2** (0.10 g, 0.13 mmol) was added a few drops of $HBF_4.Et_2O$. The mixture was swirled and the red-brown solution first turned blue, then purple and finally back to brown. The solution was stirred for 4 h and volatiles removed under vacuum to give a deep red oily solid. This was washed with a very small amount of Et_2O (to remove excess acid) and dried. Carefully layering a concentrated CH_2Cl_2 solution of **4** with Et_2O resulted in the slow formation of large red crystals of **4bb**. Data for **4bb**: IR ν(CO): 2097vs, 2048s, 2035s, 1964s cm^{-1}. $^{31}P\{^1H\}$ NMR (CD_2Cl_2): δ 55.8 (s) ppm. ^1H NMR (CD_2Cl_2): δ 7.90 –7.32 (m, 20H, Ph), 3.09 (br, 2H, CH_2), 2.58 (br, 4H, CH_2), 2.19 (t, J 13.4, 3H, Me), 1.46 (t, J 17.1, 3H, Me), –10.78 (t, J 19.2, 1H, μ-H). Elemental analysis calc. for $Fe_2S_2P_2O_4C_{34}H_{32}B_1F_4.0.5CH_2Cl_2$ (found): C 47.55 (47.86), H 3.79 (3.86). Data for **4ab**: IR ν(CO)(CH_2Cl_2): 2093vs, 2044s, 1982br cm^{-1}. $^{31}P\{^1H\}$ NMR (CD_2Cl_2): δ 68.7 (d, J 62.0), 60.1 (d, J 62.0) ppm. ^1H NMR (CD_2Cl_2): δ –15.50 (dd, J 18.4, 4.4, μ-H). Crystallographic data for **4bb**·$0.5CH_2Cl_2$: red block, dimensions 0.16 × 0.14 × 0.13 mm^3, orthorhombic, space group $Pbca$, a = 11.273(3), b = 19.387(5), c = 33.773(8) Å, α = 90, β = 90, γ = 90°, V = 7381(3) $Å^3$, Z = 8, F(000) 3544, d_{calc} = 1.567 g cm^{-3}, μ = 1.116 mm^{-1}. 59991 reflections were collected, 8946 unique [R(int) = 0.0704]. At convergence, R_1 = 0.0712, wR_2 = 0.1712 [$I > 2.0\sigma(I)$] and R_1 = 0.0877, wR_2 = 0.1791 (all data), for 460 parameters. The structure was solved using the Patterson method.

X-ray structure determinations

Single crystals of **2bb**, **3**·CH_2Cl_2, and **4**·0.5CH_2Cl_2 were mounted on glass fibres and all geometric and intensity data were taken from these samples using a Bruker SMART APEX CCD diffractometer using graphite-monochromated Mo-K_α radiation (λ = 0.71073 Å) at 150 ± 2 K. Data collection, indexing and initial cell refinements were all done using SMART [53] software. Data reduction were carried out with SAINT PLUS [54] and absorption corrections applied using the programme SADABS [55]. Structures were solved by direct methods or Patterson methods and developed using alternating cycles of least-squares refinement and difference-Fourier synthesis. All non-hydrogen atoms were refined anisotropically. Hydrogens were placed in calculated positions (riding model). Structure solution used SHELXTL PLUS V6.10 program package [56]. Crystallographic data for the structural analyses have been deposited with the Cambridge Crystallographic Data Centre, 1053582 for **2bb**, 1053616 for **3** and 1053615 for **4bb**. Copies of this information may be obtained free of charge from the Director, CCDC, 12 Union Road, Cambridge, CB2 1 EZ, UK (fax: +44-1223-336033; e-mail: deposit@ccdc.cam.ac.uk or www: http://www.ccdc.ac.uk).

Electrochemical studies

Electrochemistry was carried out in deoxygenated acetonitrile solutions with 0.1 M $TBAPF_6$ as the supporting electrolyte. The working electrode was a 3 mm diameter glassy carbon electrode that was polished with 0.3 μm alumina slurry prior to each scan. The counter electrode was a Pt wire and the quasi-reference electrode was a silver wire. All CVs were referenced to the Fc/Fc^+ redox couple. An Autolab potentiostat (EcoChemie, Netherlands) was used for all electrochemical measurements. Catalysis studies were carried out by adding measured equivalents of $HBF_4.Et_2O$ (Sigma-Aldrich).

Density functional theory (DFT) calculations

All calculations were performed with the hybrid DFT functional B3LYP, as implemented by the Gaussian 09 program package [57]. This functional utilizes the Becke three-parameter exchange functional (B3) [58], combined with the correlation functional of Lee, Yang and Parr (LYP) [59]. The iron atoms were described by Stuttgart–Dresden effective core potential (ecp) and SDD basis set, while the 6-31+G(d′) basis set was employed for the remaining

atoms. All computed species were established as intermediates or minima based on zero imaginary frequencies (positive eigenvalues). The computed frequencies were used to make zero-point and thermal corrections to the electronic energies; the reported energies are quoted in kJ mol^{-1} relative to the specified standard. The natural charges and Wiberg bond indices were computed using Weinhold's natural bond orbital (NBO) program. [60,61]. The geometry-optimized structures have been drawn with the JIMP2 molecular visualization and manipulation program [62,63].

Acknowledgements

We thank the Commonwealth Scholarship Commission for the award of a Commonwealth Scholarship to SG. MGR thanks the Robert A. Welch Foundation (grant B-1093) for financial support and acknowledges computational resources through UNT's High Performance Computing Services and CASCaM. Prof. Michael B. Hall (TAMU) is thanked for providing us a copy of his *JIMP2* program, which was used to prepare the geometry-optimized structures reported here, and Dr. David A. Hrovat (CASCam) is also thanked for help with the optimization of the radical cation **2ab**$^{\cdot+}$. GH acknowledges The Royal Society of Chemistry for an International Authors Award which allowed him to visit the University of North Texas and prepare this manuscript.

References

1 For reviews of this area see (a) I. P. Georgakaki, L. M. Thomson, E. J. Lyon, M. B. Hall, M. Y. Darensbourg, Coord. Chem. Rev. 2003, 238-239, 255-266; (b) D. J. Evans, C. J. Pickett, Chem. Soc. Rev. 2003, 32, 268-287; (c) T. B. Rauchfuss, Inorg. Chem. 2004, 43, 14-26; (d) L. Sun, B. Åkermark, S. Ott, Coord. Chem. Rev. 2005, 249, 1653-1663; (e) X. Liu, S. K. Ibrahim, C. Tard, C. J. Pickett, Coord. Chem. Rev. 2005, 249, 1641-1652; (f) C. Tard, C. J. Pickett, Chem. Rev. 2009, 109, 2245-2274; (g) J.-F. Capon, F. Gloaguen, P. Schollhammer, J. Talarmin, Coord. Chem. Rev. 2005, 249, 1664-1676. (h) M. Wang, L. Chen, X. Li, L. Sun, Dalton Trans, 2011, 40, 12793-12800.

2 J.W. Tye, M.B. Hall, M.Y. Darensbourg, Inorg. Chem., 2006, 45, 1552-1559.

3 F. I. Adam, G. Hogarth, I. Richards, B. E. Sanchez, Dalton Trans. 2007, 2495-2498.

4 F. I. Adam, G. Hogarth, I. Richards, J. Organomet. Chem. 2007, 692, 3957-3968.

5 F. I. Adam, G. Hogarth, S. E. Kabir, I. Richards, C. R. Chim. 2008, 11, 890-905.

6 S. Ghosh, G. Hogarth, N. Hollingsworth, K. B. Holt, I. Richards, M. G. Richmond, B. E. Sanchez, D. Unwin, Dalton Trans. 2013, 42, 6775-6792.

7 J.-F. Capon, F. Gloaguen, F. Y. Pétillon, P. Schollhammer and J. Talarmin, Eur. J. Inorg. Chem. 2008, 4671-4681.

8 S. Ezzaher, J.-F. Capon, F. Gloaguen, F. Y. Pétillon, P. Schollhammer, J. Talarmin, Inorg. Chem. 2007, 46, 3426-3428.

9 S. Ezzaher, J.-F. Capon, F. Gloaguen, F. Y. Pétillon, P. Schollhammer, J. Talarmin, Inorg. Chem. 2007, 46, 9863-9872.

10 S. Ezzaher, J.-F. Capon, F. Gloaguen, N. Kervarec, F. Y. Pétillon, R. Pichon, P. Schollhammer, J. Talarmin, C. R. Chim. 2008, 11, 906-914.

11 S. Ezzaher, J. -F. Capon, F. Gloaguen, F. Y. Pétillon, P. Schollhammer, J. Talarmin, N. Kervarec, Inorg. Chem. 2009, 48, 2-4.

12 S. Ezzaher, J.-F. Capon, N. Dumontet, F. Gloaguen, F. Y. Pétillon, P. Schollhammer, J. Talarmin, J. Electroanal. Chem. 2009, 626, 161-170.

13 S. Lounissi, J.-F. Capon, F. Gloaguen, F. Matoussi, F. Y. Pétillon, P. Schollhammer, J. Talarmin, Chem. Commun. 2011, 47, 878-880.

14 D. Chouffai, G. Zampella, J.-F. Capon, L. De Gioia, A. Le Goff, F. Y. Pétillon, P. Schollhammer, J. Talarmin, Organometallics 2012, 31, 1082-1091.

15 S. Lounissi, G. Zampella, J.-F. Capon, L. De Gioia, F. Matoussi, S. Mahfoudhi, F.Y. Pétillon, P. Schollhammer, J. Talarmin, Chem.-Eur. J. 2012, 18, 11123-11138.

16 C. Greco, P. Fantucci, L. De Gioia, R. Suarez-Bertoa, M. Bruschi, J. Talarmin, P. Schollhammer, Dalton Trans. 2010, 39, 7320-7329.

17 A. K Justice, G. Zampella, L. De Gioia, T. B. Rauchfuss, J. I. van der Vlugt, S. R. Wilson, Inorg. Chem. 2007, 46, 1655-1664.

18 A. K Justice, T. B. Rauchfuss, S. R. Wilson, Angew. Chem., Int. Ed. 2007, 46, 6152-6154.

19 N. Wang, M. Wang, T. Liu, T. Zhang, M. Darensbourg, L. Sun, Inorg. Chem. 2008, 47, 6948-6955.

20 N. Wang, M. Wang, J. Liu, K. Jin, L. Chen, L. Sun, Inorg. Chem. 2009, 48, 11551-11558.

21 L.-C. Song, W. Gao, X. Luo, Z.-X. Wang, X.-J. Sun, H.-B. Song, Organometallics 2012, 31, 3324-3332.

22 L.-C. Song, C.-G. Li, J.-H. Ge, Z.-Y. Yang, H.-T. Wang, J. Zhang, Q.-M. Hu, J. Inorg. Biochem. 2008, 102, 1973-1979.

23 W. Gao, J. Ekström, J. Liu, C. Chen, L. Eriksson, L. Weng, B. Åkermark, L. Sun, Inorg. Chem. 2007, 46, 1981-1991.

24 X.-F. Liu, B.-S. Yin, J. Coord. Chem. 2010, 63, 4061-4067.

25 F. Ridley, S. Ghosh, G. Hogarth, N. Hollingsworth, K. B. Holt, D. G. Unwin, J. Electroanal. Chem. 2013, 703, 14-22.

26 G. Hogarth, S. E. Kabir, I. Richards, Organometallics 2010, 29, 6559-6568.

27 S. Ghosh, G. Hogarth, N. Hollingsworth, K.B. Holt, S.E. Kabir, B.E. Sanchez, Chem. Commun. 2014, 50, 945-947.

28 M. E. Jung, G. Piizzi, Chem. Rev. 2005, 105, 1735-1766 and references therein.

29 R. M. Beesley, C. K. Ingold, J. F. Thorpe, J. Chem. Soc. 1915, 1080-1106.

30 G. Hogarth, J. Kilmartin, J. Organomet. Chem. 2007, 692, 5655-5670.

31 M. Filby, A. J. Deeming, G. Hogarth, M.-Y. Lee, Can. J. Chem. 2006, 84, 319-329.

32 (a) S. Al-Jibori, B. L. Shaw, J. Chem. Soc., Chem. Commun. 1982, 286-287; (b) Al-Jibori, B. L. Shaw, Inorg. Chim. Acta 1983, 74, 235-239.

33 W. Hewertson, N. R. Watson, J. Chem. Soc. 1962, 1490-1494.

34 J. V. Barkley, J. C. Grimshaw, S. J. Higgins, P. B. Hoare, M. K. McCart, A. K. Smith, J. Chem. Soc., Dalton Trans. 1995, 2901-2908.

35 U. Anandhi, T. Holbert, D. Leung, P. R. Sharp, Inorg. Chem. 2003, 42, 1282-1295.

36 J. V. Barkley, M. Ellis, S. J. Higgins, M. K. McCart, Organometallics 1998, 17, 1725-1731.

37 M. Ferrer, A. Gutierrez, M. Mounir, L. Rodriguez, O. Rossell, M. Font-Bardia, P. Gomez-Sal, A. Martin, X. Solans, Organometallics 2011, 30, 3419-3429.

38 J. A. van Rijn, M. A. Siegler, A. L. Spek, E. Bouwman, E. Drent, Organometallics 2009, 28, 7006-7014.

39 C. S. Kraihanzel, P. K. Maples, J. Organomet. Chem. 1976, 117, 159-170.

40 N. D. Reddy, P. E. Fanwick, R. A. Walton, Inorg. Chim. Acta 2001, 314, 189-193.

41 J. C. Sarker, A. K. Raha, S. Ghosh, G. Hogarth, S. E. Kabir, M. G. Richmond, J. Organomet. Chem. 2014, 750, 49-58.

42 A. Jablonskyté, L.R. Webster, T.R. Simmons, J.A. Wright, C.J. Pickett, J. Am. Chem. Soc. 2014, 136, 13038-13044.

43 J.A. Wright, C.J. Pickett, Chem. Commun. 2009, 5719-5721.

44 A. Jablonskyté, J.A. Wright, C.J. Pickett, Dalton Trans. 2010, 39, 3026-3034.

45 A. Jablonskyté, J.A. Wright, C.J. Pickett, Eur. J. Inorg. Chem. 2011, 1033-1037.

46 R. Zaffaroni, T.B. Rauchfuss, A. Fuller, L. De Gioia, G. Zampella, Organometallics, 2013, 32, 232-238.

47 R. Zaffaroni,T.B. Rauchfuss, D.L. Gray, L. De Gioia, G. Zampella, J. Am. Chem. Soc. 2012, 134, 19260-19269.

48 M.G.I. Galinato, C.M. Whaley, D. Roberts, P. Wang, N. Lehnert, Eur. J. Inorg. Chem. 2011, 1147-1154.

49 G. Zampella, P. Fantucci, L. De Gioia, Chem. Commun. 2010, 46, 8824-8826.

50 A. Jablonskyté, J.A. Wright, S.A. Fairhurst, J.N.T. Peck, S.K. Ibrahim, V.S. Oganesyan, C.J. Pickett, J. Am. Chem. Soc. 2011, 133, 18606-18609.

51 Mingos, D. M. P., Wales, D. J. Introduction to Cluster Chemistry; Prentice Hall: Englewood Cliffs, NJ, 1990.

52 A. Winter, L. Zsolnai, G. Huttner, Z. Naturforsch. 1982, 37b, 1430-1436.

53 SMART Version 5.628; Bruker AXS, Inc., 5465 East Cheryl Parkway, Madison, WI 53711-5373, 2003.

54 SAINT Version 6.36A; Bruker AXS, Inc., 5465 East Cheryl Parkway, Madison, WI 53711-5373, 2002.

55 G. M. Sheldrick, SADABS Version 2.10; University of Göttingen, Göttingen, Germany, 2003.

56 G. M. Sheldrick, A short history of SHELX. Acta Crystallogr. 2008, A64, 112.

57 M.J. Frisch, G.W. Trucks, H.B. Schlegel, G.E. Scuseria, M.A. Robb, J.R. Cheeseman, G. Scalmani, V. Barone, B. Mennucci, G. A. Petersson, H. Nakatsuji, M. Caricato, X. Li, H. P. Hratchian, A. F. Izmaylov, J. Bloino, G. Zheng, J.L. Sonnenberg, M. Hada, M. Ehara, K. Toyota, R. Fukuda, J. Hasegawa, M. Ishida, T. Nakajima, Y. Honda, O. Kitao, H. Nakai, T. Vreven, J.A. Montgomery Jr., J.E. Peralta, F. Ogliaro, M. Bearpark, J.J. Heyd, E. Brothers, K.N. Kudin, V.N. Staroverov, R. Kobayashi, J. Normand, K. Raghavachari, A. Rendell, J.C. Burant, S. S. Iyengar, J. Tomasi, M. Cossi, N. Rega, J. M. Millam, M. Klene, J. E. Knox, J. B. Cross, V. Bakken, C. Adamo, J. Jaramillo, R. Gomperts, R. E. Stratmann, O. Yazyev, A. J. Austin, R. Cammi, C. Pomelli, J. W. Ochterski, R. L. Martin, K. Morokuma, V. G. Zakrzewski, G. A. Voth, P. Salvador, J. J. Dannenberg, S. Dapprich, A. D. Daniels, O. Farkas, J. B. Foresman, J. V. Ortiz, J. Cioslowski, D. J. Fox, GAUSSIAN 09 (Revision A.02), Gaussian, Inc., Wallingford, CT, 2009.

58 A.D. Becke, J. Chem. Phys. 1993, 98, 5648-5652.

59 C. Lee, W. Yang, R. G. Parr, Phys. Rev. B: Condens. Matter 1988, 37, 785-789.

60 A. E. Reed, L. A. Curtiss, F. Weinhold, Chem. Rev. 1988, 88, 899-926.

61 K. B. Wiberg, Tetrahedron 1968, 24, 1083-1096.

62 JIMP2, version 0.091, a free program for the visualization and manipulation of molecules: M. B. Hall, R. F. Fenske, Inorg. Chem. 1972, 11, 768-775.

63 J. Manson, C. E. Webster, M. B. Hall, Texas A&M University, College Station, TX, 2006, http://www.chem.tamu.edu/jimp2/index.html.

Table 1. Selected natural charges and Wiberg bond indices for the different Fe_2(μ-pdt)(diphosphine) compounds[a]

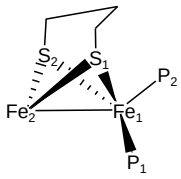

2bb

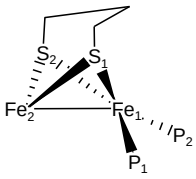

2ab

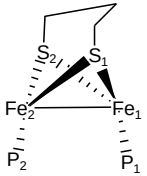

3

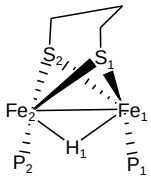

4bb

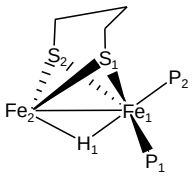

$Fe_2(H)^n$

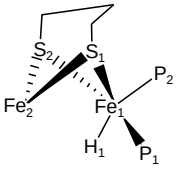

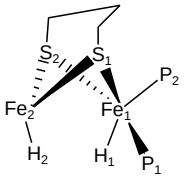

$Fe_2(H)_2$

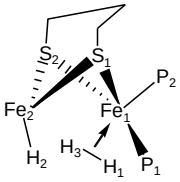

$Fe_2(H)(H_2)^+$

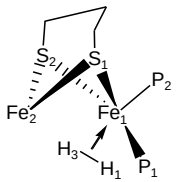

$Fe_2(H_2)^+$

Atomic Charge	**2bb**	**2ab**	**3**	**$2ab^{-+}$**	**4bb**	**$Fe_2(H)^+$**	**$Fe_2(H)$**	**$Fe_2(H)^-$**	**$Fe_2(H)_2$**	**$Fe_2(H)(H_2)^+$**	**$Fe_2(H_2)^+$**
Fe_1	-1.38	-1.33	-1.57	-0.60	-1.46	-1.39	-1.49	-1.63	-1.52	-1.29	-1.36
Fe_2	-1.66	-1.65	-1.57	-1.36	-1.69	-1.69	-1.52	-1.53	-1.83	-1.77	-1.30
P_1	1.31	1.28	1.37	1.15	1.37	1.32	1.32	1.35	1.35	1.32	1.33
P_2	1.33	1.32	1.34	1.14	1.34	1.36	1.25	1.23	1.22	1.31	1.35
S_1	0.34	0.29	0.39	0.24	0.39	0.36	0.23	0.18	0.25	0.27	0.23
S_2	0.35	0.30	0.32	0.26	0.38	0.36	0.24	0.16	0.29	0.29	0.24
H_1					0.19	0.19	0.18	0.20	0.14	0.16	0.19
H_2									0.22	0.13	0.17
H_3										0.19	

Table 1. Con't.

Wiberg index	**2bb**	**2ab**	**3**	**2ab$^{\cdot+}$**	**4bb**	**$Fe_2(H)^+$**	**$Fe_2(H)$**	**$Fe_2(H)^-$**	**$Fe_2(H)_2$**	**$Fe_2(H)(H_2)^+$**	**$Fe_2(H_2)^+$**
Fe-Fe	0.44	0.46	0.47	0.20	0.29	0.30	0.16	0.06	0.04	0.04	0.07
Fe-P_1	0.75	0.74	0.77	0.60	0.78	0.77	0.77	0.79	0.79	0.79	0.78
Fe-P_2	0.75	0.77	0.77	0.57	0.78	0.79	0.66	0.64	0.66	0.77	0.79
Fe_1-S_1	0.80	0.76	0.78	0.72	0.77	0.75	0.69	0.70	0.66	0.73	0.74
Fe_2-S_1	0.75	0.74	0.79	0.72	0.78	0.79	0.69	0.66	0.74	0.75	0.70
Fe_1-S_2	0.81	0.77	0.76	0.68	0.77	0.74	0.71	0.74	0.70	0.73	0.73
Fe_2-S_2	0.73	0.73	0.76	0.74	0.79	0.78	0.67	0.56	0.74	0.74	0.70
Fe_1-H_1					0.34	0.35	0.54	0.72	0.75	0.30	0.28
Fe_2-H_1					0.46	0.45	0.23	0.02			
Fe_2-H_2									0.69	0.73	
Fe_1-H_3										0.29	0.29
H_1-H_3										0.59	0.59

[a]Atom orientation and numbering scheme for the Fe_2 compounds depicted above. Only selected atoms are shown.